WS06 B01

Tomographic model uncertainties and their effect on imaged structures.

M. Reinier* (CGG), J. Messud (CGG), P. Guillaume (CGG), T. Rebert (CGG)

Summary

We demonstrate a recently developed method for computing tomography model uncertainties and mapping them into the migrated domain. After the final tomography, the method generates a series of equi-probable velocity model perturbations within a standard deviation confidence level. This allows computing standard deviation-like attributes for velocity and anisotropy parameters and for key horizons. An application to West of Shetland dataset highlights the interest of the estimated uncertainties.

Introduction

Seismic imaging is a common technique and a basis for well planning, reserve estimation and production optimization. The accuracy of seismic reflector positioning greatly depends on the migration "velocity" model (including anisotropy). The related uncertainties have only been investigated recently (Osypov et al., 2013) but they are crucial for reservoir risk analysis. Indeed, the migration velocity model directly affects lateral and vertical positioning of migrated structures.

Messud et al. (2017; 2017b) have proposed a strategy aiming at assessing structural uncertainties associated with ray-based tomography. After the final tomography step, the method generates a series of equi-probable velocity model perturbations that are both tomographically-consistent and within a confidence level defined by standard deviation. In a second step, standard deviation-like attributes are computed for key horizons before being combined with well information in order to carry out reservoir risk analysis or other studies.

The method is applied to a West of Shetland marine dataset recently reprocessed (Toubiana et al., 2017). We first briefly describe the applied tomography-based velocity model building workflow. The results of the uncertainty analysis presented here relate to velocity, ε parameters (that are jointly estimated) and migrated key horizons.

Pre-uncertainty analysis tomography workflow

The dataset consists of two merged marine acquisitions from the 90's, and reprocessed in 2016 using the latest broadband processing technology. A two-pass depth velocity model building workflow involving Tilted Transverse Isotropic (TTI) nonlinear slope tomography (Guillaume et al., 2013) has been applied. Each pass includes a pre-stack migration, a dense volumetric Residual Move-Out (RMO) picking on computed common image gathers (CIGs) and a nonlinear depth tomography. The TTI symmetry axis follows the layering. In the first tomography pass, V_p (velocity along TTI axis) is updated by inverting RMO information picked from pre-stack time migration CIGs (Lambaré et al., 2007). A global well calibration is then performed using available well markers to mainly re-balance V_p and δ model parameters for each layer. In the second multi-layer tomography pass, V_p and ε are simultaneously updated (preserving well-ties) to produce a maximum likelihood TTI velocity model that best minimizes RMO. The right-hand part of Figure 1 illustrates the decrease of tomography cost function after each pass of nonlinear tomography.

From ray-based tomography to velocity uncertainty analysis

Uncertainties relating to velocity model parameters can be evaluated by developing a probability density function (PDF) around the model obtained by final tomography which is assumed to be maximum likelihood model. The method proposed by Messud et al. (2017b) assumes the PDF has a Gaussian distribution in a sufficiently large interval. Starting with the tomographic system, the developed method computes equi-probable velocity model perturbations that are within a 68.3% (or standard deviation) confidence level. Uncertainty attributes can then be computed statistically using the obtained perturbations, involving map (or zero-offset kinematic) migrations in perturbed models.

The tomography "cost function" values shown in Figure 1 are computed from the "data term": root mean square of the RMO weighted by a quality factor (the "constraints (or regularization) term" being most often small at the maximum likelihood by construction of our inversion scheme). Within the frame of non-linear slope tomography the cost functions related to the perturbations can be estimated automatically and non-linearly (Messud et al., 2017b). Figure 1 displays the cost function values obtained for the 46 first equi-probable velocity perturbations (out of 500). We observe that the cost function values computed for all perturbed models are almost identical, thus confirming that the PDF was sampled along an almost equi-probable contour, giving almost equi-probable velocity models. This allows the geophysicist to check the pertinence of the method.

Model perturbations are applied simultaneously to V_p and ε parameters and they are computed for all estimated velocity grid parameters. The final tomography TTI model is shown in Figures 2a and 2b. The model perturbations generated by the algorithm depend on the grid mesh sizes on which the

parameters are estimated: V_p grid mesh was chosen 2 to 4 times smaller than ε grid mesh. The first computed model perturbations are shown in Figure 2c for V_p and Figure 2d for ε.

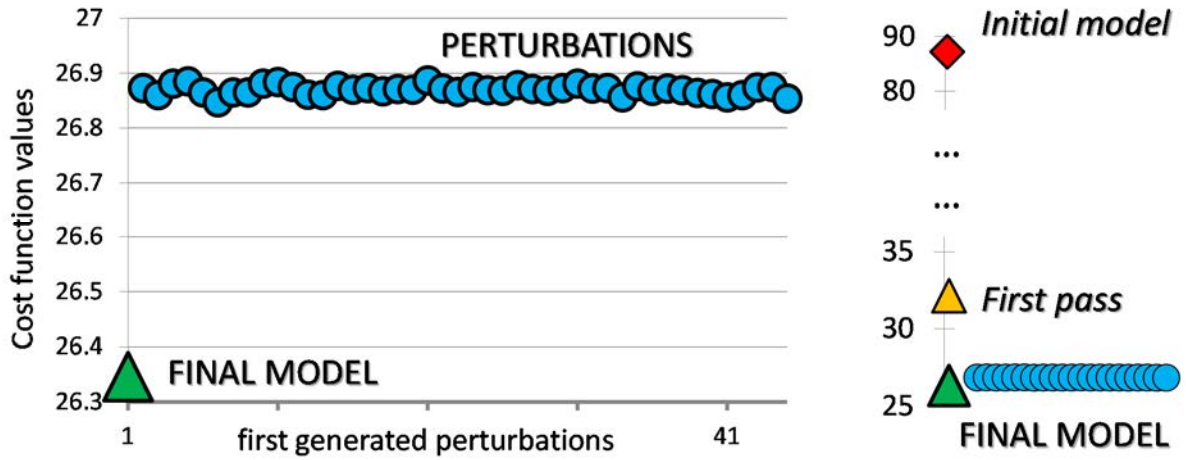

Figure 1: *Left: Tomography cost function values for final TTI model (i.e. maximum likelihood model) and the 46 first generated perturbed models among 500. Right: Cost function values after each velocity model building phase, represented with a larger nonlinear scale.*

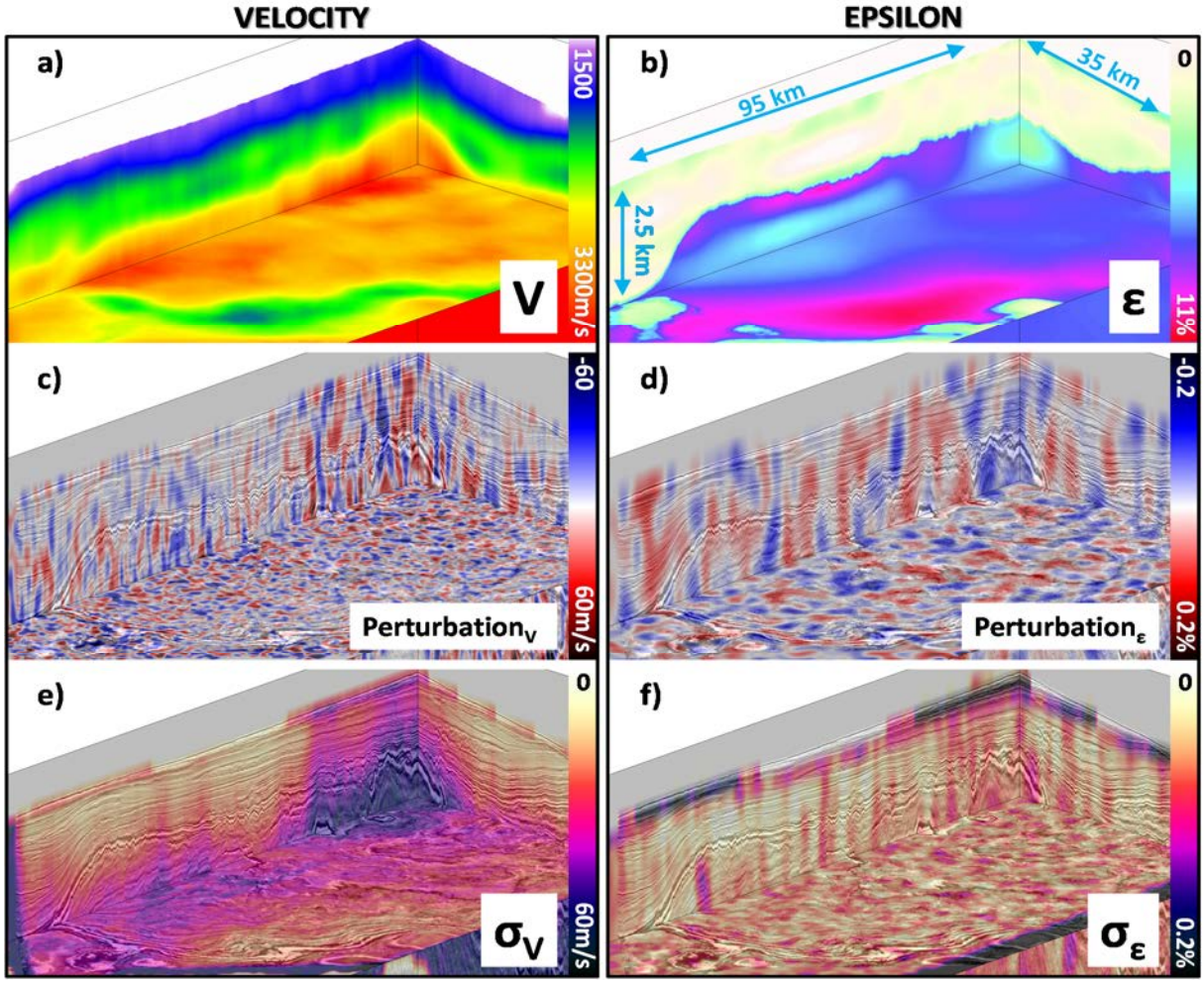

Figure 2: ***a)*** *Final V_p model;* ***b)*** *Final ε model;* ***c)*** *First V_p perturbation among 500;* ***d)*** *First ε perturbation among 500;* ***e)*** *V_p standard deviation σ_V computed from 500 V_p perturbations;* ***f)*** *ε standard deviation $\sigma_ε$ computed from 500 ε perturbations.*

Error bars on V_p and ε model parameters can be computed considering the maximum possible variations of the perturbations (Messud et al., 2017b). Since the perturbations are related to a standard

deviation confidence level, the error bars are referred to as "standard deviation-like attribute", here represented by σ. The V_p standard deviation σ_V increases with depth and lateral changes show much longer spatial wavelengths (Figure 2e) than the ε standard deviation σ_ε (Figure 2f).

Tomographic model uncertainties can also be mapped into the migrated domain. For this purpose, target horizons are zero-offset re-migrated in each perturbed model where both V_p and ε are simultaneously perturbed. A standard-deviation-like attribute on the depth position of each horizon is thus derived (Messud et al., 2017; Messud et al., 2017b).

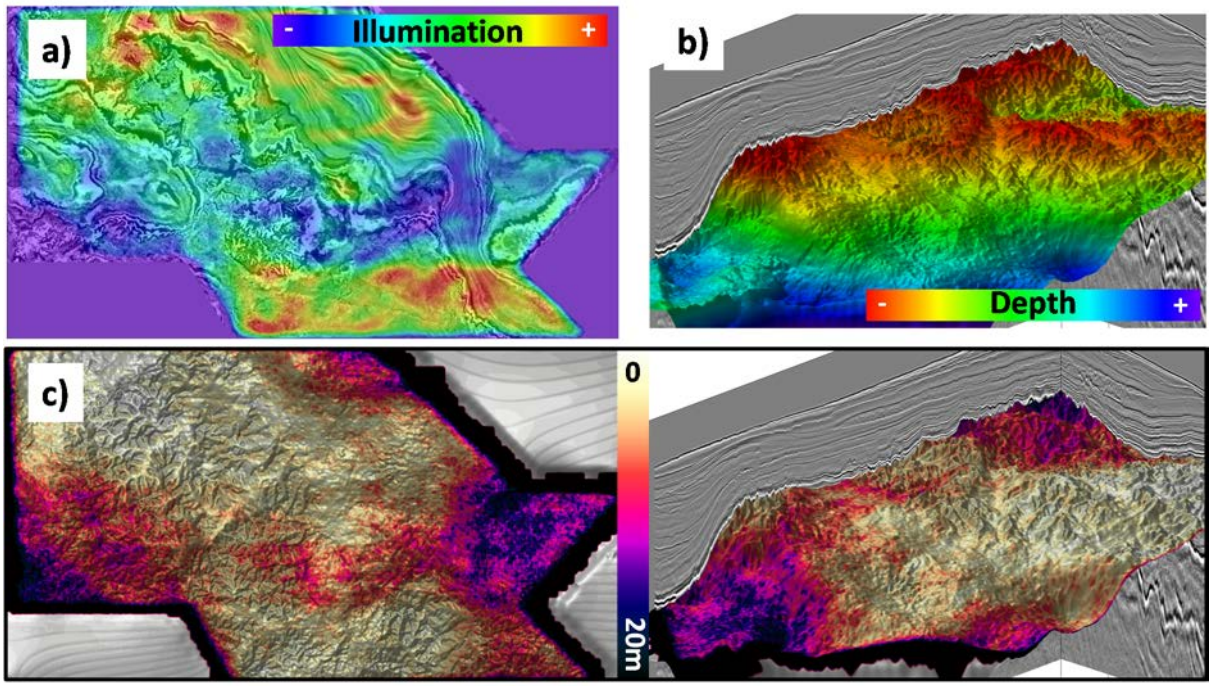

Figure 3: *Base Flett horizon.* ***a)*** *Illumination map overlaying seismic depth slice at 1700m;* ***b)*** *Depth attribute in 3D view;* ***c)*** *Depth standard deviation attribute σ_Z in meters, in map and 3D views.*

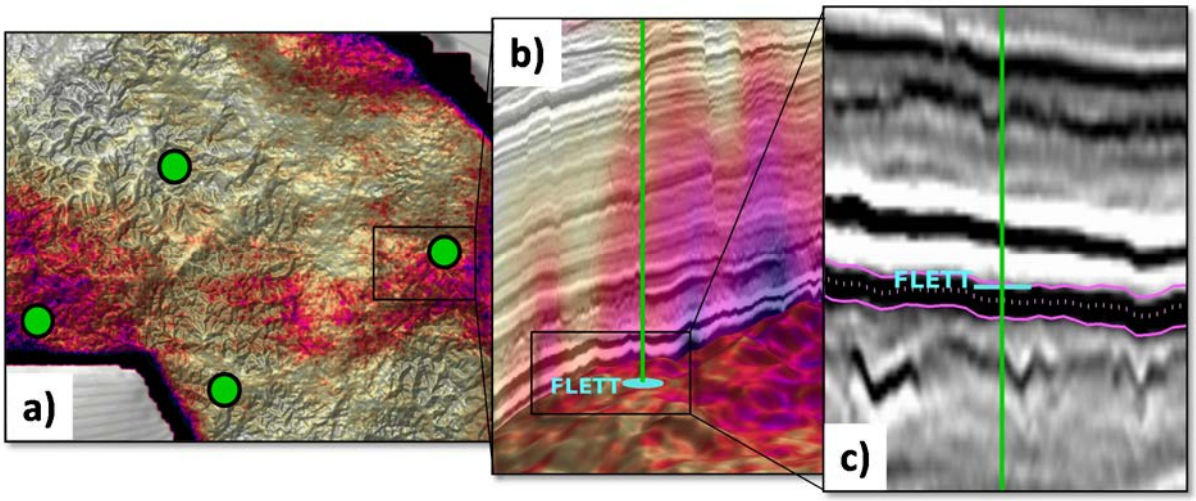

Figure 4: a) *Horizon depth standard deviation map with 4 well locations (green dots);* ***b)*** *3D zoom-in around one well with Base Flett marker (cyan) and migrated seismic overlaid with V_p standard deviation σ_V in the background;* ***c)*** *Seismic imaged section, Base Flett marker (cyan), Base Flett horizon (pink dotted line) and envelope of horizon depth positions defined by bounding pink horizon lines.*

The geological horizon Base Flett around 2000m depth (Figure 3), chosen for its structural complexity, illustrates the estimate of uncertainty on horizon depth position. Horizon depth standard deviation increases with depth and structural dips (Figure 3c). Figures 3a and 3c show that the

uncertainty hierarchy is nicely correlated with variations in illumination. Areas with weaker illumination in blue on Figure 3a, corresponding to changes of mixed acquisition surveys and to depth variations of seabed, correlate with higher uncertainty areas in red on Figure 3c.

An uncertainty analysis limited to V_p perturbations produces similar standard deviations of the horizon depth, indicating that uncertainties are mostly driven by V_p errors.

The uncertainty analysis results can be matched with well data (Figure 4). The four wells shown in Figure 4a are located in areas with different hierarchies of horizon depth uncertainty. A closer look at the well in Figure 4b shows that horizon depth uncertainties have high lateral variability but nicely follow the V_p standard deviation σ_V. These uncertainties are also correlated to fault offsets clearly visible on the seismic. Figure 4c shows that the Base Flett marker (in cyan color) does not perfectly match the imaged seismic event identified by the pink dotted line (centre of the black trough). Instead, it lies within the computed error bars represented by the horizon depth "envelope" in purple color: the observed residual mis-ties are explained by the fact that the final model tries to honour both the picked RMO field and the layer-based well calibration constraints. Interestingly, the horizon error bars (or depth "envelope") tend to wrap around the Base Flett seismic wavelet.

Conclusions

We showed a method for computing tomography uncertainties and mapping them into the migrated domain. For that purpose, equi-probable V_p and ε model perturbations are generated. It provides a smart method for sampling the PDF, assuming Gaussian shape. Nonlinear tomography makes it possible to efficiently compute the cost function in each perturbed model, thus allowing the geophysicist to check the equi-probability of computed model perturbations and thus the pertinence of the method. The application to real data highlights the three dimensional variability of the estimated uncertainties. The horizon standard deviation resulting from simultaneous V_p and ε perturbations is calculated and compared to both well marker information and seismic wavelet to provide control points. As the error bars tend to wrap around the seismic event wavelet, the logical next step would be to use them to guide the image well calibration away from wells. This methodology can be applied in the context of well prognosis so that geologists and drillers can better quantify uncertainties around the depth of reservoir targets.

Acknowledgements

The authors are grateful to CGG Multi-Client & New Ventures Division for permission to show and publish these results. We also thank Sylvie Baillon, Hélène Toubiana, Guillaume Gigou and Lilas Vivin having performed the data re-processing.

References

Guillaume, P., Zhang, X., Prescott, A., Lambaré, G., Reinier, M, Montel, J-P and Cavalié, A. [2013] Multi-layer non-linear slope tomography. *75th EAGE Conference & Exhibition*, Extended Abstracts, Th 04 01.

Lambaré, G., Herrmann, P., Touré, J. P., Capar, L., Bousquié, N., Grenié, D. and Zimine, S. [2007] From time to depth imaging – A fast and accurate workflow, *77th EAGE Conference & Exhibition*, Extended abstracts, C006.

Messud, J., Reinier, M., Prigent, H., Guillaume, P., Coléou, T. and Masclet, S. [2017] Extracting seismic uncertainties from tomographic velocity inversion and their use in reservoir risk analysis. *The Leading Edge*, February 2017.

Messud, J., Guillaume, P. and Lambaré, G. [2017b] Estimating structural uncertainties in seismic images using qui-probable tomographic models. *Submitted to 79th EAGE Conference & Exhibition*.

Osypov, K., Yang, Y., Fournier, A., Ivanova, N., Bachrach, R., Yarman, C. E., You, Y., Nichols, D. and Woodward, M. [2013] Model-uncertainty quantification in seismic tomography: method and applications, *Geophysical Prospecting*, 61, no. 6, 1114-1134.

Toubiana, H., Gigou, G., Vivin, L., Rebert, T., Baillon, S., Rivault, JL., Palmer, J., Krishna, H. and James, G. [2017] Reviving old seismic data using latest broadband processing technology: a case study from West Of Shetland. *Submitted to 79th EAGE Conference & Exhibition*.